**ORIGINAL PAPER**

# An improved nonlinear creep damage model of slates considering freeze–thaw damage and bedding damage

Xiurong Yang[1] · Annan Jiang[1]

## Abstract

To study the creep behavior of bedding slates after freezing and thawing, the RLW-2000 rock creep triaxial instrument was used to carry out the creep test, and the creep curves of slate under different bedding angles and different freeze–thaw cycles were obtained. Then, based on the slate creep test results and the fractional-order theory, a new nonlinear creep damage model considering freeze–thaw damage and bedding damage was proposed. The creep damage model can not only describe the changes in the three creep stages (primary creep, steady-state creep, and accelerated creep) but also reflect the influence of freeze–thaw and bedding coupling damage on creep characteristics. The mathematical optimization analysis software 1stOpt was used to identify the parameters of the nonlinear creep damage model. Finally, the influence of stress level and bedding angle on creep parameters was analyzed, and the creep characteristic parameters in the creep damage model were sensitively analyzed. The consistency between the test data and the predicted results showed that the nonlinear creep damage model proposed in this study can accurately reflect the creep behavior of rock with freeze–thaw and bedding-damaged.

**Keywords** Bedding slate · Creep characteristics · Freeze–thaw (F-T) cycles · Fractional derivative · Creep damage model

## Introduction

The freezing and thawing of rock and soil is a natural phenomenon in cold regions. The repeated freeze–thaw action gradually leads to the deterioration of rock mechanical properties, which causes great harm to the construction of geotechnical engineerings, such as slipping of the open-pit mining slopes, cracking and collapsing of tunnel linings, frost heave deformation of railway subgrades, and deterioration of geotechnical materials (Ghobadi and Babazadeh 2015; Jin 2010; Kawamura and Miura 2013; Knutsson et al. 2018). In addition, the existence of weak planes (i.e., bedding, jointing, layering, flaw, and fissuring et al.) in the rock mass is quite common in nature (Lee and Pietruszczak 2008; Zhang et al. 2019b), and the strength characteristics of anisotropic rocks are also related to the bedding planes orientation (Fu et al. 2018). The existence of bedding planes will aggravate

the development of rock freeze–thaw damage (Zhang et al. 2019a). One of the most important mechanical properties of rocks creep properties is a key factor affecting the design, working life, safety, and stability of underground caverns in bedding slate (Cornet and Dabrowski 2018). Therefore, it is of great significance to study the creep characteristics of bedding slates after freezing and thawing to improve the safety of rock engineering projects in cold regions.

The effect of freezing and thawing on the mechanical properties of rocks is a topic of particular concern to researchers (Hale and Shakoor 2003; Jia et al. 2019; Khanlari et al. 2015; Sun et al. 2020; Yang et al. 2010; Yavuz 2011). Wang et al. (2016) studied the influence of freeze–thaw cycles on static compression and dynamic impact experiments of red sandstone and used a decay model to describe the reduction of rock strength with the increasing number of freeze–thaw weathering cycles. The effects of freeze–thaw cycles on mechanical characteristics of the Gödene stone in Konya (Turkey) were investigated by Gökçe et al. (2016). The greatest factor during the freeze–thaw process was the existence of water. The water contained in the body (in discontinuities and pores) of a building stone freezes along with the fall of temperature below 0 °C. Besides, the effect of freeze–thaw action on the durability of rocks was

✉ Annan Jiang
  jiangannan@163.com

  Xiurong Yang
  yangxiurong6@163.com

1  Institute of Road and Bridge Engineering, Dalian Maritime University, Dalian 116026, Liaoning, China

more severe in sodium sulfate solution as compared with freshwater (Jamshidi et al. 2016). Yang et al. (2019) studied the time-dependent behavior of quartz sandstone and quartzite in four different chemical solutions (acidic HCl solution, neutral NaCl solution, alkaline NaOH solution, and distilled water) after freezing and thawing. The elastic modulus of quartzite is the most damaged after HCl solution corrosion, followed by NaOH, NaCl, and pure water turn. Wang et al. (2021) conducted a shear creep test on red sandstone in a freeze–thaw environment, analyzed the shear creep characteristics of rocks in different temperature ranges, and established the Burgers model considering freeze–thaw cycle and damage. Kodama et al. (2019) conducted a series of uniaxial compression and creep tests on dry and wet samples of tuff under low-temperature conditions (-20℃) and studied the time dependence of the mechanical behavior of frozen rocks. Yang et al. (2021) analyzed and discussed the influence of freeze–thaw cycles on the creep characteristics of saturated gneiss and, based on the test results, proposed a variable parameter model that considers the creep damage of the freeze–thaw cycles on the gneiss.

In recent years, many scholars have studied the creep characteristics of rocks (Bai et al. 2021; Feng et al. 2020; Hou et al. 2018; Liu et al. 2020; Wang et al. 2019). Multi-stage loading triaxial creep test was performed on the cataclastic rock, and the creep mechanical behavior of the rock was studied (Zhang et al. 2016). Rassouli and Zoback (2018) conducted a series of long-term creep experiments on horizontal and vertical shale samples rich in clay and carbonate. Hu et al. (2019) performed a cyclic loading and unloading creep test on the artificially layered cemented samples and defined time-independent (instantaneous elasticity and instantaneous plasticity) and time-dependent (viscoelastic and viscoplastic) deformations. Based on the test results, many scholars believe that there is a significant coupling characteristic between rock damage and creep and proposed a corresponding creep damage model (Hou et al. 2018; Ma et al. 2017; Wang et al. 2019; Zhang et al. 2009). Zhou et al. (2011) replaced the Newtonian damper in the classical Nishihara model with the Abel damper and proposed a creep constitutive model based on the fractional derivative. Bai et al. (2021) established a nonlinear viscoelastic-plastic constitutive model of red sandstone with a single ice crack based on the fractional calculus theory and Kachanov damage theory. Feng et al. (2020) improved the Nishihara model and established a nonlinear creep damage model considering initial damage and damage evolution. Wang et al. (2019) combined the theory of continuous damage mechanics and used elastic modulus to characterize rock damage, and established a constitutive model of salt rock creep damage. Based on the multi-stage loading creep test of sandstone with different initial damage degrees, Hou et al. (2018) proposed a new non-linear creep damage model of rock. Cong and Hu (2017) conducted a

triaxial creep test on sandstone under low confining pressure and established an improved Burgers model to describe initial creep and steady creep. Zhang et al. (2020a) analyzed the influence of freeze–thaw cycles on the mechanical properties of water-saturated rocks, combined with rheological theory, and proposed an elastic-visco-plastic model based on the stress function. Kuhn and Mitchell (1992) proposed the rate process theory (RPT) and used the discrete element method (DEM) to simulate the soil creep process. Gutiérrez-Ch et al. (2021) used the DEM combined with RPT to simulate the rock response in the creep stage of slate.

The above research results well illustrate the rock creep mechanism, but mainly focus on the creep behavior of homogeneity rock mass under indoor temperature, lacking the research on the creep behavior of rock mass under freeze–thaw cycles, especially the freeze–thaw bedding rock. Although the creep model of rock materials has been improved in recent years, most general models cannot fully describe the creep characteristics of bedding slates after freezing and thawing. Therefore, this study conducted triaxial compression creep tests on bedding slate samples with different freeze–thaw cycles. Then, based on freeze–thaw and bedding coupling damage and fractional calculus theory, a creep constitutive model considering freeze–thaw damage and bedding damage was established. Then, the influence of stress level and bedding angle on creep parameters was analyzed. Through the sensitivity analysis of the creep characteristic parameters, the rationality of the creep damage model proposed in this study was verified. This study can be used to evaluate the long-term stability of bedding tunnels and bedding slopes in cold areas and provide a theoretical basis for the support design of tunnels and slopes.

# Experimental procedures

## Experimental material

This study takes the bedding slate as the research object. The slate samples are taken from a tunnel project in a seasonal frozen area in northern China. X-ray diffraction (XRD) analysis (Fig. 1) indicated that the slate used in this study was composed of quartz, mica, calcite, and other clay minerals. According to the test specification recommended by the International Society for Rock Mechanics (ISRM), the standard cylindrical sample with a diameter of 50 mm and a height of 100 mm was prepared. The non-parallelism of both ends of the sample was controlled within $\pm 0.02$ mm, as shown in Fig. 2a. The basic physical and mechanical parameters of the slate sample are presented in Table 1, and the curves of the uniaxial compressive strength tests are in Fig. 3. The dry density of the slate is 2.71 g/cm$^3$, the natural water content is 0.45%, the saturated water content is 1.69%,
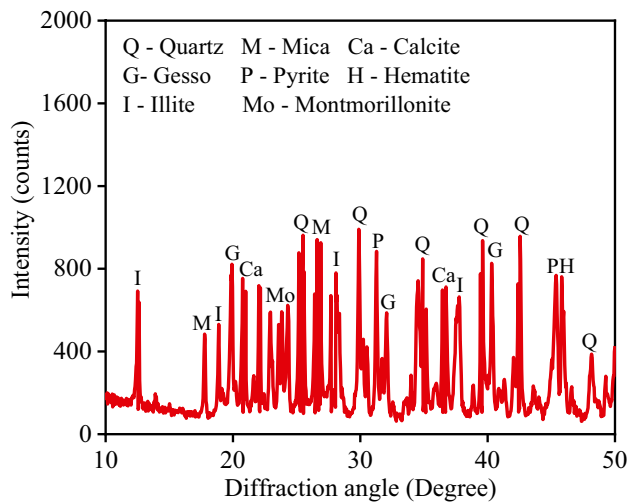
**Fig. 1** X-ray diffraction (XRD) analysis

and the porosity is 3.25%. For each bedding orientation (0°, 30°, 45°, 60°, and 90°), 10 samples were prepared. In total, 50 samples were prepared, and each set of bedding orientation samples was divided into 5 groups, with 2 samples per group. Each group was subjected to a different number of F-T cycles, i.e., 0, 20, 40, 60, and 80 cycles.

## Experimental equipment and program

1. Freeze–thaw cycle tests

   The appearance, control panel, and internal structure of the freeze–thaw equipment are shown in Fig. 2b. The device has a sinusoidal and linear (including constant temperature)

**Table 1** The physical and mechanical parameters of the slate

| Bedding angle (°) | Mean P-wave velocity (m•s$^{-1}$) | Uniaxial compressive strength (MPa) | Elastic modulus (GPa) | Poisson ratio |
|---|---|---|---|---|
| 0 | 5625 | 161.70 | 60.83 | 0.27 |
| 30 | 5431 | 68.90 | 37.26 | 0.22 |
| 45 | 5394 | 79.14 | 45.09 | 0.21 |
| 60 | 5440 | 77.41 | 42.74 | 0.24 |
| 90 | 5728 | 170.25 | 73.19 | 0.31 |

regular compound programming capability, which is suitable for F-T cycles ranging from −70 °C to 150 °C. The digital screen displays the set temperature and actual temperature. The temperature uniformity is less than 2.0 °C, whereas the temperature deviation is within ± 2.0 °C.

This study considers the freeze–thaw cycle (−20 °C –20 °C) as the external environmental conditions of the sample. Each F-T cycle is set as 12 h (–20 ℃ for 6 h, 20 ℃ for 6 h), and the number of F-T cycles is set as 0, 20, 40, 60, and 80 times, respectively. Before the freeze–thaw cycle tests, the prepared sample is saturated in the saturator for 120 h; then the sample is taken out and put into the water container and then put into the freeze–thaw equipment for the freeze–thaw cycle. As the critical degree of saturation has an important influence on the freeze–thaw damage of the rock (Al-Omari et al. 2015), the samples always maintain a saturated state during the freeze–thaw process.

2. Triaxial compression creep test
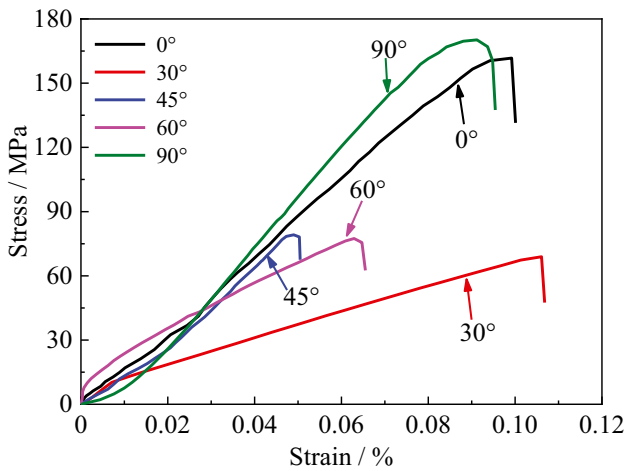
**Fig. 2** Experimental equipment
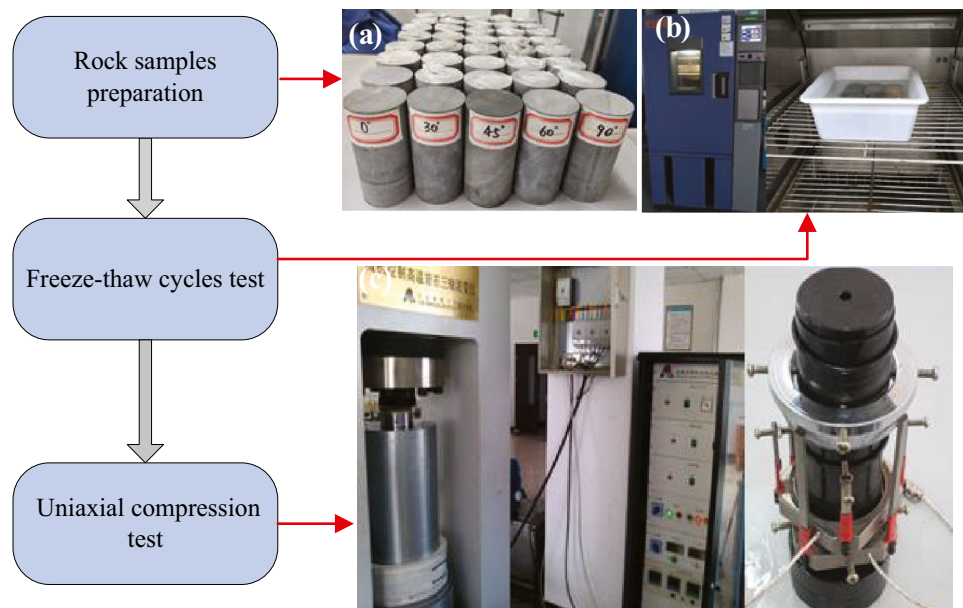
**Fig. 3** Curves of slate uniaxial compressive strength under different bedding angles

The multi-functional RLW-2000 rock triaxial apparatus developed by Dalian Maritime University is used for the uniaxial compression test. The test equipment is shown in Fig. 2c. The equipment can be used for a full stress–strain test and rheological test under high and low temperature, high pore pressure, and permeability environment. The full digital servo control, ball screw, and hydraulic technology produced by the German DOLI company can control osmotic pressure, confining pressure, and axial pressure stably. The maximum confining pressure is 80 MPa, and the maximum osmotic pressure is 60 MPa. The control accuracy is within $\pm 0.01\%$.

According to the survey data, the ground stress of the tunnel is that the maximum horizontal principal stress is 4.83 MPa—5.74 MPa, and the minimum horizontal principal stress is 4.29 MPa—4.87 MPa. This test only studied the mechanical properties of the bedding slate under the confining pressure of 5 MPa in the above stress range. Table 2 shows the triaxial compression creep test program for bedding slate samples. The axial load was applied at a constant rate of 0.5 MPa/min until the loading was stopped at predetermined axial stress (Chen et al. 2018). Due to the large dispersion of strength of slate with different bedding angles, the initial loading axial stress of the sample is different. During a

**Table 2** Testing program of loading creep

| Property | Slate | | | | |
|---|---|---|---|---|---|
| Bedding angle (°) | 0 | 30 | 45 | 60 | 90 |
| Initial value $\sigma_1$ (MPa) | 10 | 10 | 10 | 10 | 10 |
| $\Delta\sigma$ (MPa) | 20 | 5 | 10 | 10 | 20 |
| Confining pressure $\sigma_3$ (MPa) | 5 | | | | |

multi-loading triaxial creep test, four to seven levels of axial stress were applied. The minimum holding time for each loading step was 24 h, and the creep strain rate of the sample was less than 0.001 mm/h.

## Experimental results and analysis

### Creep deformation

The axial strain–time curve of the slate sample under different bending angles and different freeze–thaw cycles is shown in Fig. 4. It can be seen from Fig. 4 that the creep characteristics of the sample are related to the freeze–thaw cycles, bedding angles, and axial stress. Taking the sample with $\beta = 0°$ as an example, it can be seen from Fig. 4a that when the axial stress is 10 MPa, the instantaneous elastic strains are 0.0094%, 0.0155%, 0.0209%, 0.0283%, and 0.0357%, respectively, for the samples after freeze–thaw 0, 20, 40, 60 and 80 cycles, and the creep strains are 0.0288%, 0.0381%, 0.0495%, 0.0579%, and 0.0692%, respectively. The samples after freeze–thaw 0, 20, 40, 60, and 80 cycles experienced creep failure at 110 MPa, 110 MPa, 90 MPa, 90 MPa, and 90 MPa, respectively. It can be seen from the above that, under a certain stress level, the instantaneous elastic strain and creep strain of the sample both increase with the increase of the freeze–thaw cycles. However, the creep failure stress of the samples decreases with the increase of the freeze–thaw cycles.
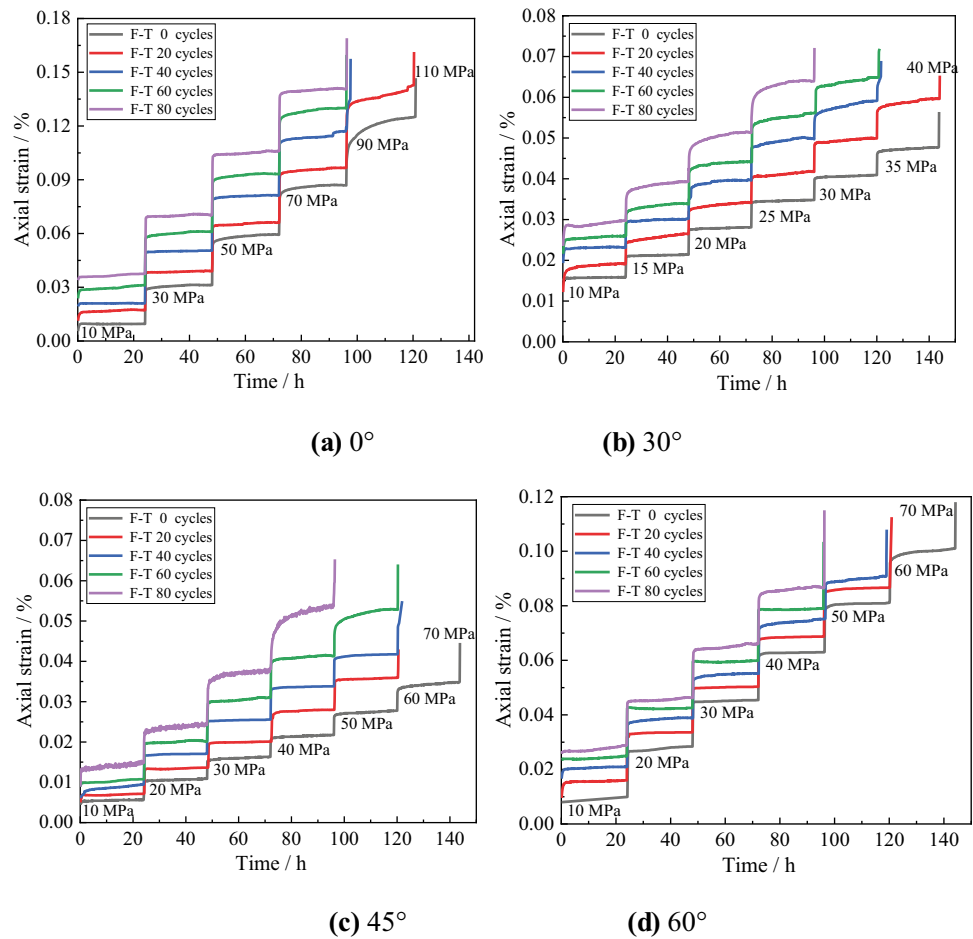
The slate sample produces instantaneous strain at the moment when the stress is applied, and creep strain occurs under long-term stress. Under the action of the first-level loading stress, the creep deformation of the sample is obvious. The slope of the creep curve increases with increasing stress. The creep curve shows a deceleration creep stage and steady-state creep stage. The creep behavior of the slate sample becomes more and more obvious when the stress continues to be applied. When loaded to the last level of stress, the axial strain of the sample gradually increases with time, showing the typical three stages of rock creep behavior, that is, the primary creep stage, steady-state creep stage, and accelerated creep stage. And the sample failure occurs in the accelerated creep stage. Under certain stress levels, with the increase of freeze–thaw cycles, the instantaneous strain and creep strain of bedding slate increase, and the creep curve changes gradually to steep.

In addition, the axial strain–time curve of the 80 F-T cycles slate under different bedding angles is shown in Fig. 5. Under certain freeze–thaw cycles, the creep characteristics of the sample are related to the bedding angles and axial stress. It can be seen from Fig. 5 that the failure stress of samples with $\beta = 0°$, 30°, 45°, 60° and 90° are 90, 30, 50,

**Fig. 4** Curves of slate creep test under different freeze–thaw cycles



**(a)** 0°

**(b)** 30°



**(c)** 45°

**(d)** 60°

50, and 90 MPa, respectively. With the increase of the bedding angle, the failure stress of the sample first decreased and then increased, which is similar to the law of uniaxial compressive strength.
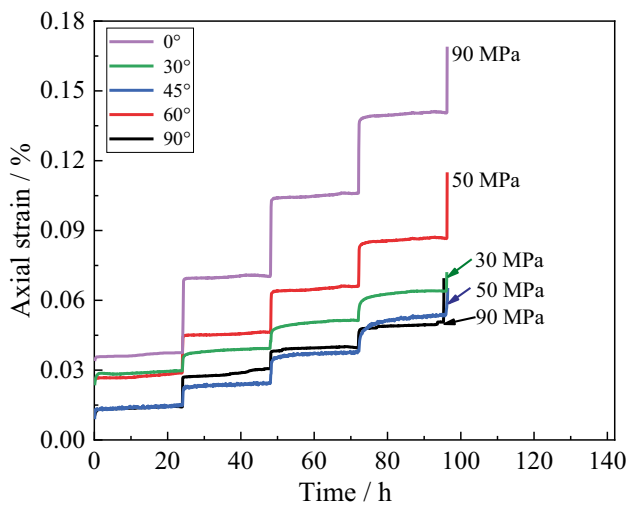


**Fig. 5** Curves of slate creep test under different bedding angles (80 F-T cycles)

## Creep strain rate

The creep rate is an important indicator reflecting the performance of the creep curve. Under the last stage load, the slate samples with different freeze–thaw cycles and different bedding angles experienced creep failure. The relationship curve between the axial strain rate and time in the creep test is determined by calculating the slope of the creep curve. Figure 6 shows the curves of axial strain and strain rate with the time of slate sample with different bedding angles under 80 F-T cycles.

It can be seen from Fig. 6 that the slate sample develops from steady-state creep to acceleration creep after deceleration creep, and then failure occurs in the acceleration creep stage. The duration of the deceleration creep stage and acceleration creep stage is shorter than that of the steady-state creep stage.

Taking the sample with $\beta = 45°$ as an example, it can be seen from Fig. 6c that the strain rate of the sample decreased from $0.733 \times 10^{-2}$ /h to $0.017 \times 10^{-2}$ /h and then stabilized in the $AB$ region, which is the primary creep stage. In the $BC$ region of the creep curve, when the strain rate is $0.017 \times 10^{-2}$ /h, the strain rate remains unchanged and the axial strain

**(a)** 0°



**(b)** 30°



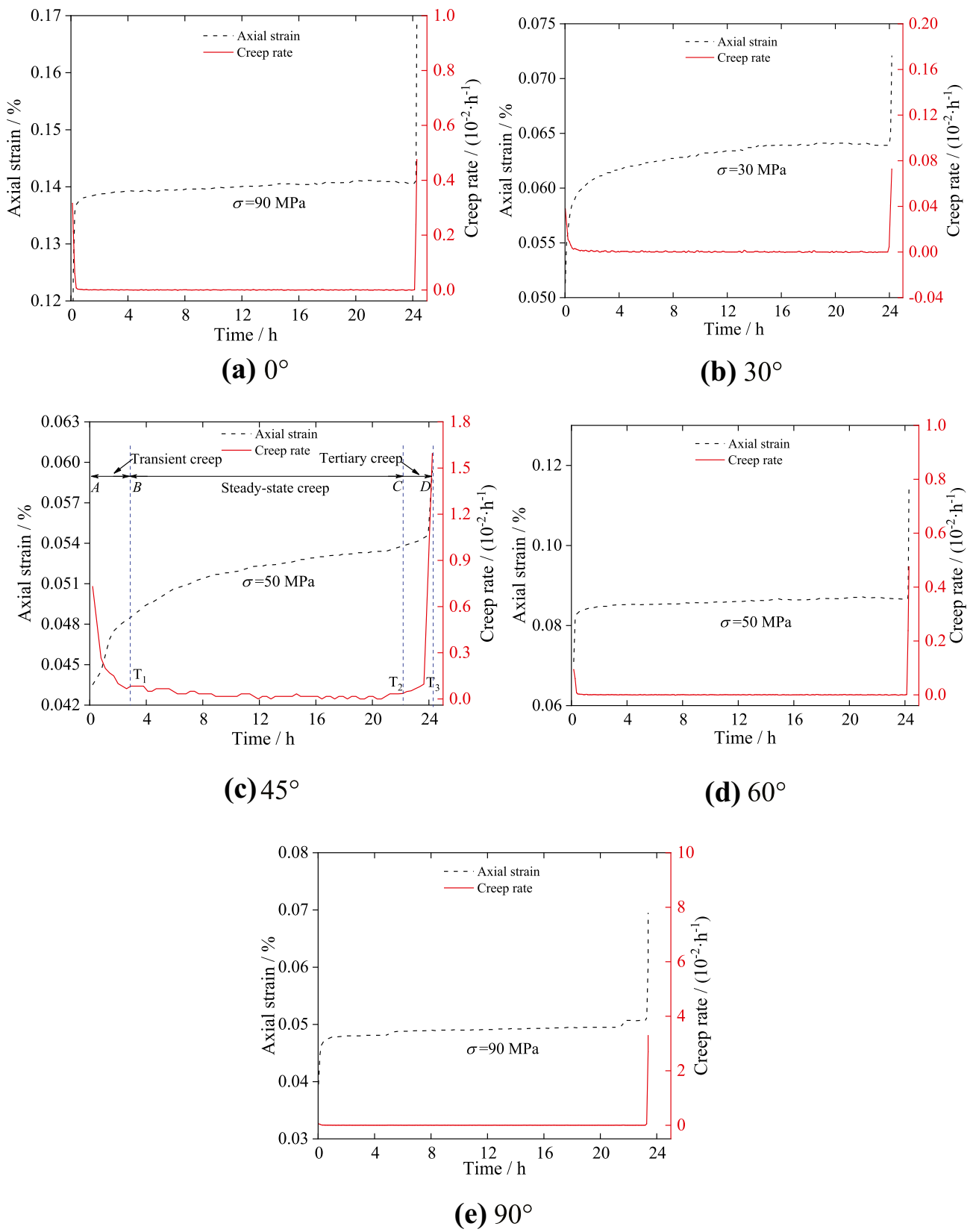**(c)** 45°



**(d)** 60°



**(e)** 90°

**Fig. 6** The axial strain rate of the slate sample under 80 F-T cycles versus time

increases slightly, which is considered the steady-state creep stage. In the *CD* region, the strain rate increases sharply until the rock failure, which can be regarded as the accelerated creep stage. Therefore, the creep characteristics of the bedding slate have obvious time-dependent characteristics. The creep process includes three classical stages: initial creep stage (*AB*), steady-state creep stage (*BC*), and accelerated creep stage (*CD*) (Boukharov et al. 1995; Main 2010; Ngwenya et al. 2001).

In Fig. 6c, $T_1$ (5.89 h) is used as the primary creep limit, and $T_2$ (22.3 h) and $T_3$ (23.6 h) are used as the start time and end time of accelerated creep. The primary creep, steady-state creep, and accelerated creep times are 5.89 h, 19.28 h, and 1.3 h, respectively. In the long-term steady-state creep stage, the cumulative creep strain increases with time. When the cumulative creep strain is greater than the steady-state creep limit strain, the sample will enter the accelerated creep stage. During the accelerated creep stage, the axial strain and the strain rate suddenly increase, which indicates that as the microcracks in the specimen expand and propagate, creep failure eventually occurs.

The failure stress, creep duration, and creep rate of the slate with $\beta = 45°$ under different freeze–thaw cycles were compared, as shown in Table 3. The creep rate of the sample increases with the increase of the number of freeze–thaw cycles. For the sample after freeze–thaw 0 cycles, the initial creep rate, steady-state creep rate, and accelerated creep rate are $0.408 \times 10^{-2} \cdot h^{-1}$, $0.0106 \times 10^{-2} \cdot h^{-1}$, and $1.073 \times 10^{-2} \cdot h^{-1}$, respectively, while for the sample after 80 F-T cycles, they are $0.733 \times 10^{-2} \cdot h^{-1}$, $0.0170 \times 10^{-2} \cdot h^{-1}$, and $1.597 \times 10^{-2} \cdot h^{-1}$, respectively. With the increase in freeze–thaw cycles, the failure stress and creep duration of the sample decrease gradually. Creep failure occurred at 70 MPa for the sample after freeze–thaw 0 cycles, and the creep duration is 143.80 h. With the increase in freeze–thaw cycles, the failure stresses of the samples after freeze–thaw 20, 40, 60, and 80 cycles are 60 MPa, 60 MPa, 60 MPa, and 50 MPa, respectively, and the creep duration is 121.91 h, 120.51 h, 119.31 h, and 96.45 h, respectively.

In addition, the creep rate curve of slate under different freeze–thaw cycles and different bedding angles is shown in Fig. 7. Taking the sample with $\beta = 45°$ as an example, it can be seen from Fig. 7a that the initial creep rate and accelerated creep rate increase with the increase of freeze–thaw cycles, but the steady creep rate does not change much. The steady creep rates under different freeze–thaw cycles are all close to 0. Taking the sample with F-T 80 cycles as an example, as the bedding angles increases, the initial creep rate and accelerated creep rate first increase and then decrease, but the steady creep rate does not change much, as shown in Fig. 7b. The variation law of the initial creep rate and the accelerated creep rate of the sample may be related to the bedding structure of the rock.

## Creep damage model

It can be seen from the above that the damage caused by the freeze–thaw cycles and the bedding angles affects the creep mechanical properties and creep parameters of the slate. Therefore, it is necessary to carry out research using a creep damage constitutive model that considers the freeze–thaw cycles and bedding angle.

Fractional calculus is a branch of mathematics that studies the possibility of considering the power law of real or complex differential and integral operators. Fractional calculus can solve the problem in mathematical modeling. Compared with integer calculus, the theoretical model of fractional calculus is in good agreement with experimental results. Fractional calculus uses fewer parameters and more concise expression, so it has been applied in many fields. In recent years, fractional calculus has been gradually developed in the field of rock rheology, and fractional calculus is often defined by Riemann–Liouville's theory. Riemann–Liouville's fractional derivative takes the derivation of a constant, and the result is not zero (Kilbas et al. 2006). In addition, in the field of rock creep constitutive models, the Riemann–Liouville fractional calculus operator theory is the most widely used (Liu et al. 2020). For the *m*-order Riemann–Liouville integral of function $f(t)$, as shown in Eq. (1):

**Table 3** Creep rate of slate under failure stress ($\beta = 45°$)

| F-T cycles | Failure stress (MPa) | Creep duration (h) | Failure strain (%) | Long-term strength (MPa) | Primary creep — Initial creep rate ($10^{-2} \cdot h^{-1}$) | Steady-state creep — Steady creep rate ($10^{-2} \cdot h^{-1}$) | Accelerated creep — Accelerated creep rate ($10^{-2} \cdot h^{-1}$) |
|---|---|---|---|---|---|---|---|
| 0 | 70 | 143.80 | 0.042 | 65.42 | 0.408 | 0.0106 | 1.073 |
| 20 | 60 | 121.91 | 0.045 | 58.29 | 0.491 | 0.0114 | 1.184 |
| 40 | 60 | 120.51 | 0.055 | 55.70 | 0.560 | 0.0139 | 1.292 |
| 60 | 60 | 119.31 | 0.064 | 51.63 | 0.642 | 0.0158 | 1.436 |
| 80 | 50 | 96.45 | 0.066 | 47.31 | 0.733 | 0.0170 | 1.597 |

**(a)** $\beta=45°$

**(b)** F-T cycles=80
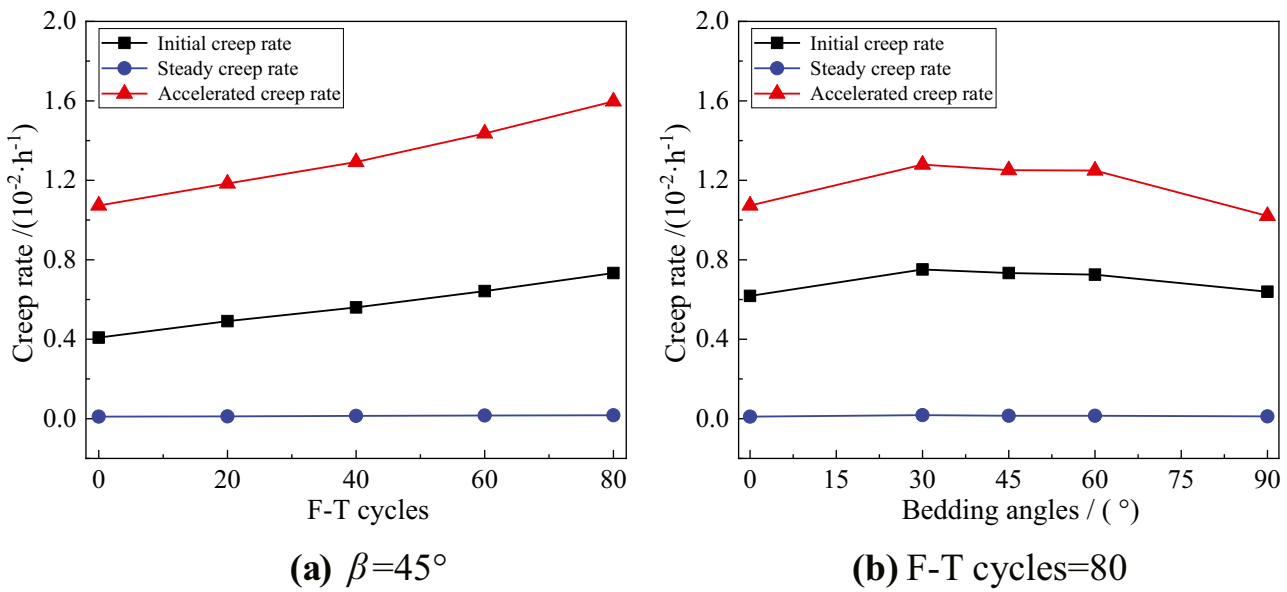
**Fig. 7** Creep rate of slate under different freeze–thaw cycles and different bedding angles

$$\frac{d^{-m}[f(t)]}{dt^{-m}} = D_t^{-m}f(t) = \frac{1}{\Gamma(m)} \int_0^t (t-\xi)^{m-1} f(\xi) d\xi \qquad (1)$$

The fractional differential is shown in Eq. (2):

$$\frac{d^m f(t)}{dt^m} = D_t^m f(t) = \frac{d^k}{dt^k} \left[ D_t^{-(k-m)} f(t) \right] \qquad (2)$$

where $\Gamma(m)$ is the Gamma function, $\Gamma(m) = \int_0^\infty t^{m-1} e^{-t} dt$, $k$ is a positive integer, $m$ is the fractional order and $m$ lies between $0 \leq m \leq 1$.

The fractional derivative is applied to the rheological model (Kelvin and Maxwell) by replacing the damper with the spring. The ideal solid (spring) follows Hooke's law, and the Newtonian fluid (damper) follows Newton's viscosity law (Kabwe et al. 2020; Yin et al. 2013).

## Soft-matter element

The stress–strain relationship of the ideal solid satisfies Hooke's law, and the ideal fluid satisfies Newton's viscosity law. Therefore, the stress–strain characteristics of geotechnical materials between ideal solid and ideal fluid can be expressed by soft-matter element (Abel dashpot), as shown in Fig. 8 (Zhou et al. 2011).

The stress versus strain relationship of the soft-matter element can be calculated according to Eq. (3):

$$\sigma(t) = \eta \frac{d^m \varepsilon(t)}{dt^m} \qquad (3)$$

where $\eta$ is the viscosity coefficient of the soft-matter element. $m$ is the fractional order and $m$ lies between $0 \leq m \leq 1$. Equation (3) can be reduced to Hooke's elastic law when $m$ is 0 and similarly to Newton's fluid law when $m$ is 1. The soft-matter element can describe stress versus strain characteristics between ideal elastic and fluid materials when $m$ is between 0 and 1. The soft-matter element can describe the accelerated creep state of the rock when $m$ is greater than 1.

The creep constitutive equation of the soft-matter element can be obtained using the Riemann–Liouville fractional differential operator theory, as shown in Eq. (4):

$$\varepsilon(t) = \frac{\sigma}{\eta} \frac{t^m}{\Gamma(1+m)} \qquad (4)$$

The creep rate of the Abel dashpot element can be obtained from the derivation of Eq. (4), as shown in Eq. (5):

$$\dot{\varepsilon}(t) = \frac{\sigma}{\eta} \frac{m t^{m-1}}{\Gamma(1+m)} dt \qquad (5)$$

Equation (5) is a decreasing function when $m$ is between 0 and 1. That is, the strain rate decreases continuously in the creep process, which can describe the deceleration creep
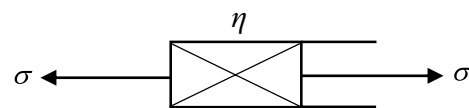


**Fig. 8** Soft-matter element

characteristics of rock materials. Equation (5) is an increasing function when $m$ is greater than 1, which describes the accelerated creep characteristics. Equation (5) can be transformed into Eq. (6) when $m$ is 1:

$$\dot{\varepsilon}(t) = \frac{\sigma}{\eta} \tag{6}$$

Equation (4) shows that when $m$ is 1, the strain rate $\dot{\varepsilon}(t)$ is constant, which can describe the steady-state creep characteristics of rock materials.

Equation (4) denotes the creep strain characterized by the Abel dashpot. Substituting $\sigma = 30$ MPa and $\eta = 3$ GPa·h into Eq. (4), one finds a series of creep curves under the cases of different derivative orders $m$ (Fig. 9), showing the dependence of creep strain on the derivative order.

Figure 9a shows that for an $m$ value between 0 and 1, the strain versus time curves gradually increase, although the growth rate slows gradually, which describes the steady-state creep characteristics of the geomaterials. In addition, the growth rate of the creep curves increases significantly when $m$ is greater than 1 (Fig. 9b), which in turn describes the accelerated creep characteristics.

## Bedding, freeze–thaw, and load coupling damage

According to the creep test results of slate with different bedding angles and different freeze–thaw cycles, the bedding, and freeze–thaw coupling damage was introduced. A nonlinear viscoelastic plastic creep model considering the coupling damage of freeze–thaw and bedding was established to describe the creep mechanical properties of slate.

According to Lemaitre's strain equivalence principle, the strain caused by the action of total stress $\sigma$ on the damaged material is equivalent to that caused by the action of effective stress $\sigma'$ on the non-damaged material.

$$\varepsilon = \frac{\sigma}{E'} = \frac{\sigma'}{E} \tag{7}$$

where $E$ and $E'$ are the elasticity modulus of non-damaged rock and damaged rock, respectively.

At present, there is no mature method to reflect the influence of bedding angle in the creep model of bedding rock. Some scholars regard bedding as a kind of damage in the rock mechanics model (Shi et al. 2020; Zhang et al. 2021). Therefore, this study tries to introduce rock bedding into the creep model in the form of a damage variable.

According to Eq. (7), the bedding angles damage variable $D_\beta$ of slate is defined as

$$D_\beta = 1 - \frac{E_\beta}{E_0} \tag{8}$$

where $\beta$ is the bedding angle, $E_\beta$ is the elastic modulus of the slate sample with bedding angle $\beta$, and $E_0$ is the elastic modulus of the slate sample with bedding angle $\beta = 0°$.

The freeze–thaw damage variable $D_n$ of slate is defined as (Zhang et al. 2020b)

$$D_n = 1 - \frac{E_n}{E} \tag{9}$$

where $n$ is the freeze–thaw cycles, $E_n$ is the elastic modulus of the slate sample at certain bedding angles after freeze–thaw $n$ cycles, $E$ is the elastic modulus of an unfrozen and thawed slate sample at certain bedding angles.

The total damage variable of rock with bedding angles under freeze–thaw cycles was obtained from Eqs. (8) and (9).

$$D_{\beta n} = D_\beta + D_n - D_\beta D_n \tag{10}$$

Equation (10) characterizes the nonlinear relationship between the two types of damage caused by bedding angles and freeze–thaw cycles and total damage. The

**Fig. 9** Creep curves of soft-matter element ($\sigma = 30$ MPa, $\eta = 3$ GPa·h)
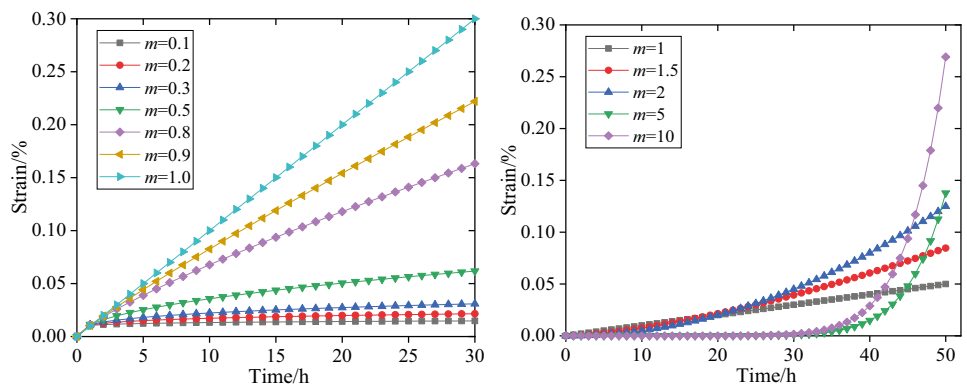


**(a)** $0 < m \leq 1$                    **(b)** $m \geq 1$

coupling effect of the two types of damage has a weakening effect on total damage.

In addition, when the applied load reaches or exceeds certain axial stress, load damage will occur inside the rock, so the influence of load damage on creep parameters should also be considered (Yang et al. 2021). Since the load damage in the two stages of deceleration creep and steady-state creep is relatively small, this study only considers the damage caused by the stress in the accelerated creep. The load damage $D_s$ is:

$$D_s = 1 - e^{-\alpha t} \tag{11}$$

According to Eqs. (8), (9), and (11), the coupling damage of bedding damage, freeze–thaw damage, and load damage at the accelerated stage can be expressed as

$$D_{\beta ns} = D_\beta + D_n + D_s - D_\beta D_n - D_\beta D_s - D_n D_s + D_\beta D_n D_s \tag{12}$$

Figure 10 shows the creep curves of rock at different stress levels, and Fig. 11 shows the nonlinear creep model considering bedding, freeze–thaw, and load coupling damage. Combined with the classical creep model (Maxwell, Kelvin, and Binham model) and the above-improved creep components, a nonlinear viscoelastic plastic creep model considering the bedding and freeze–thaw coupling damage was established, as shown in Fig. 11.

### Instantaneous elastic deformation component

In the rock creep test, when the stress level is less than the long-term strength of the rock, the sample will produce instantaneous strain during the loading process. Since the loading time is shorter than the later creep time, the sample can be considered that the elastic strain is instantaneously completed. The Hooke body is used to describe
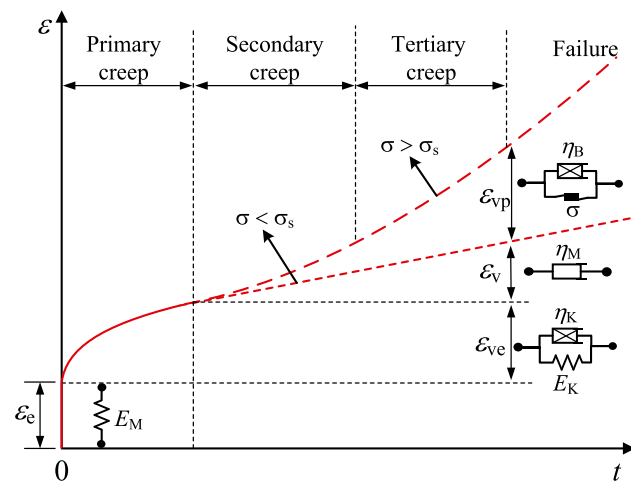
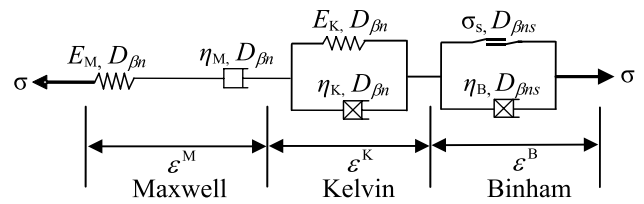**Fig. 10** Creep curve of rock under different stress levels

**Fig. 11** Nonlinear creep model considering bedding, freeze–thaw, and load coupling damage

the instantaneous elastic deformation of the rock, and the constitutive relation is given by

$$\varepsilon_M = \frac{\sigma'}{E_M} \tag{13}$$

where $\varepsilon_M$, $E_M$ are the strain and elasticity modulus of the Hooke body, respectively. $\sigma'$ is deviatoric stress.

### New nonlinear visco-elasticity component

The strain rate of rock gradually decreases and approaches 0 at last. Therefore, the strain curve in the decay creep stage has obvious nonlinear characteristics. The main reason for the model is that the parameters of the model are constant and do not change with time. In this paper, the modified Kelvin model is used to express the nonlinear characteristics of the rock creep curve, that is, the software element is parallel with the Hooke body to describe the decay creep deformation of rock. According to the series–parallel relationship, it can be obtained that:

$$\begin{cases} \varepsilon_K = \varepsilon_H = \varepsilon_N \\ \sigma' = E_K \varepsilon_K + \eta_K \dfrac{d^{m_1} \varepsilon_K(t)}{dt^{m_1}} \end{cases} \tag{14}$$

where $\varepsilon_H$, $\varepsilon_N$ are the strain of the Hooke body and the strain of the soft-matter element, respectively. $E_K$, $\varepsilon_K$ are the elasticity modulus and strain of the Kelvin body, respectively. $\sigma'$ is deviatoric stress, $\eta_K$ is the viscosity coefficient of the soft-matter element, $m$ is the fractional order and $m$ lies between $0 \leq m \leq 1$.

Equation (6) can be rewritten as

$$\frac{\sigma'}{\eta_K} = \frac{E_K}{\eta_K} \varepsilon_K + \frac{d^{m_1} \varepsilon_K(t)}{dt^{m_1}} \tag{15}$$

Considering an initial condition $\varepsilon_K(t) = 0$ when time $t = 0$, and suppose $a = E_K/\eta_K$, $b = \sigma'/\eta_K$, Eq. (15) can be rewritten as

$$b = a\varepsilon_K + \frac{d^{m_1} \varepsilon_K(t)}{dt^{m_1}} \tag{16}$$

Based on the theory of fractional calculus (Kilbas et al. 2006), the relationship between the Riemann–Liouville fractional derivative and the Caputo fractional derivative $^C D_t^m f(t)$ is given by

$$D_t^m f(t) = {}^C D_t^m f(t) + \sum_{k=0}^{n-1} \frac{t^{k-m} f^{(k)}(0)}{\Gamma(1+k-m)} \quad (0 < m < n) \quad (17)$$

Considering an initial condition $\varepsilon_K(0) = 0$, one gets $D^m[\varepsilon_K(t)] = {}^C D^m[\varepsilon_K(t)]$, then Eq. (16) can be rewritten as

$$b = a\varepsilon_K + {}^C D^m[\varepsilon_K(t)] \quad (18)$$

Taking a Laplace transform on both sides of Eq. (18), we get

$$\frac{b}{s} = aE(s) + s^m E(s) \quad (19)$$

i.e.,

$$E(s) = \frac{b}{s(s^m + a)} \quad (20)$$

Taking Laplace inverse transform on Eq. (20), we get

$$\varepsilon_K(t) = b \int_0^t (t-s)^{m-1} E_{m,m}[-a(t-s)^m] ds \quad (21)$$

where

$$E_{m,m}(x) = \sum_{k=0}^{\infty} \frac{x^k}{\Gamma(km+m)} \quad (22)$$

It can be further given by

$$\varepsilon_K = b \sum_{k=0}^{\infty} \frac{(-a)^k t^{m_1(1+k)}}{m_1(1+k)\Gamma[m_1(1+k)]} \quad (23)$$

Substituting $a = E_K/\eta_K$ and $b = \sigma/\eta_K$ into Eq. (21), we obtain the general solution:

$$\varepsilon_K = \frac{\sigma}{\eta_K} \sum_{k=0}^{\infty} \frac{(-(E_K/\eta_K))^k t^{m_1(1+k)}}{m_1(1+k)\Gamma[m_1(1+k)]} \quad (24)$$

where $k$ is a positive integer, $m_1$ is the fractional order and $m_1$ lies between $0 \le m_1 \le 1$.

## Viscous rheological component

When the stress level is close to the long-term strength of the rock, the strain of the rock is linear with time after the deceleration creep stage, and the stress–strain relationship in this process is described by the viscous body. Newton's

body is used to describe the steady-state creep deformation of rock, and the constitutive relation is given by

$$\sigma' = \dot{\varepsilon}_v \eta_M \quad (25)$$

where $\dot{\varepsilon}_v$ is the strain rate of the Newton body, $\sigma'$ is deviatoric stress, $\eta_M$ is the viscosity coefficient of the Newton body.

## Nonlinear visco-plasticity component

When the stress level exceeds the long-term strength of the rock, the rock passes through the deceleration creep stage and the steady-state creep stage and quickly enters the acceleration creep stage. In the acceleration creep stage, the strain and strain rate increase rapidly, and the nonlinear characteristics of the strain curve are obvious. When $m$ is greater than 1, the strain of the soft-matter element increases significantly with time, showing the characteristics of accelerated creep, and the creep characteristics gradually increase with the increase of the $m$ value. Therefore, the viscoplastic element with soft-matter element and plastic slider in parallel can be used to describe the viscoplastic deformation of rock, to better reflect the accelerated creep stage of rock.

According to the principle of parallel connection of elements in Fig. 11, the stress–strain relationship of the Binham body can be obtained as follows

$$\varepsilon_B = \begin{cases} 0 & , \sigma < \sigma_s \\ \dfrac{\sigma' - \sigma_s}{\eta_B} \dfrac{t^{m_2}}{\Gamma(1+m_2)} & , \sigma \ge \sigma_s \end{cases} \quad (26)$$

where $\eta_B$ is the viscosity coefficient of the Binham body, $m_2$ is the fractional order and $m_2$ lies between $0 \le m_2 \le 1$. $\sigma_s$ is the long-term strength of the slate, which can be obtained experimentally.

## Nonlinear creep damage model

According to Fig. 11, the components of the nonlinear creep damage model satisfy the following equations

$$\left.\begin{array}{l} \sigma = \sigma_M = \sigma_K = \sigma_B \\ \varepsilon = \varepsilon_M + \varepsilon_K + \varepsilon_B \\ \sigma_M = E_M(1 - D_{\beta n})\varepsilon_e = \eta_M(1 - D_{\beta n})\dot{\varepsilon}_v \\ \sigma_K = E_K(1 - D_{\beta n})\varepsilon_K + \eta_K(1 - D_{\beta n})\dfrac{d^{m_1}\varepsilon(t)}{dt^{m_1}} \\ \sigma_B = \eta_B(1 - D_{\beta ns})\dfrac{d^{m_2}\varepsilon(t)}{dt^{m_2}} + \sigma_s(1 - D_{\beta ns}) \end{array}\right\} \quad (27)$$

where $\sigma$, $\varepsilon$ are the total stress and total strain, respectively. $\sigma_M$, $\sigma_K$, $\sigma_B$ are the stress on Maxwell's body, Kelvin's body, and Binham's body, respectively. $\varepsilon_M$, $\varepsilon_K$, $\varepsilon_B$ are the strain of Maxwell's body, Kelvin's body, and Binham's body, respectively.

The creep model considering freeze–thaw and bedding coupling damage shown in Fig. 11 is given by

$\beta = 0°$ as an example, when the stress levels are 10, 30, and 50 MPa, the test curve is characterized by the deceleration creep stage, and the formula under the conditions $\sigma' < \sigma_s$ in Eq. (28) is used for fitting. When $\sigma' \geq \sigma_s$, the rock enters the accelerated creep stage, the formula under the condition $\sigma' \geq \sigma_s$ of Eq. (28) is used for fitting. In addition, the long-term strength ($\sigma_s$) of rock mass is an important indica-

$$\varepsilon = \begin{cases} \dfrac{\sigma}{E_M(1-D_{\beta n})} + \dfrac{\sigma}{\eta_M(1-D_{\beta n})}t + \dfrac{\sigma}{\eta_K(1-D_{\beta n})}\displaystyle\sum_{k=0}^{\infty}\dfrac{(-(E_K/\eta_K))^k t^{m_1(1+k)}}{m_1(1+k)\Gamma[m_1(1+k)]} & , \sigma < \sigma_s \\[3em] \dfrac{\sigma}{E_M(1-D_{\beta n})} + \dfrac{\sigma}{\eta_M(1-D_{\beta n})}t + \dfrac{\sigma}{\eta_K(1-D_{\beta n})}\displaystyle\sum_{k=0}^{\infty}\dfrac{(-(E_K/\eta_K))^k t^{m_1(1+k)}}{m_1(1+k)\Gamma[m_1(1+k)]} + \dfrac{\sigma'-\sigma_s(1-D_{\beta ns})}{\eta_B(1-D_{\beta ns})}\dfrac{t^{m_2}}{\Gamma(1+m_2)}, \sigma \geq \sigma_s \end{cases} \tag{28}$$

## Model verification

### Parameter identification and validation of test results

Adopt the Boltzmann superposition principle (Landel and Nielsen 1993) to process the creep curve. Based on the experimental results, the universal global optimization algorithm in the mathematical optimization analysis software 1stOpt is used to carry out a regression analysis of the model in this paper, and the optimal model parameter values are determined. Taking the creep test of slate with

tor of long-term stability and safety considering the time-dependent behavior (Damjanac and Fairhurst 2010). The steady-state creep rate method was used for data analysis in this study. The parameter $\sigma_s$ and the creep parameter identification results are shown in Table 4. The fitting curve of the triaxial creep test of slate samples with different bedding angles after undergoing 80 freeze–thaw cycles is shown in Fig. 12.

Figure 12 shows the comparison between the creep test curve and fitting curve of the theoretical model of slate samples with different bedding angles after undergoing 80 freeze–thaw cycles. Table 4 shows that the theoretical

**Table 4** Creep damage model parameters under different conditions (F-T cycles = 80)

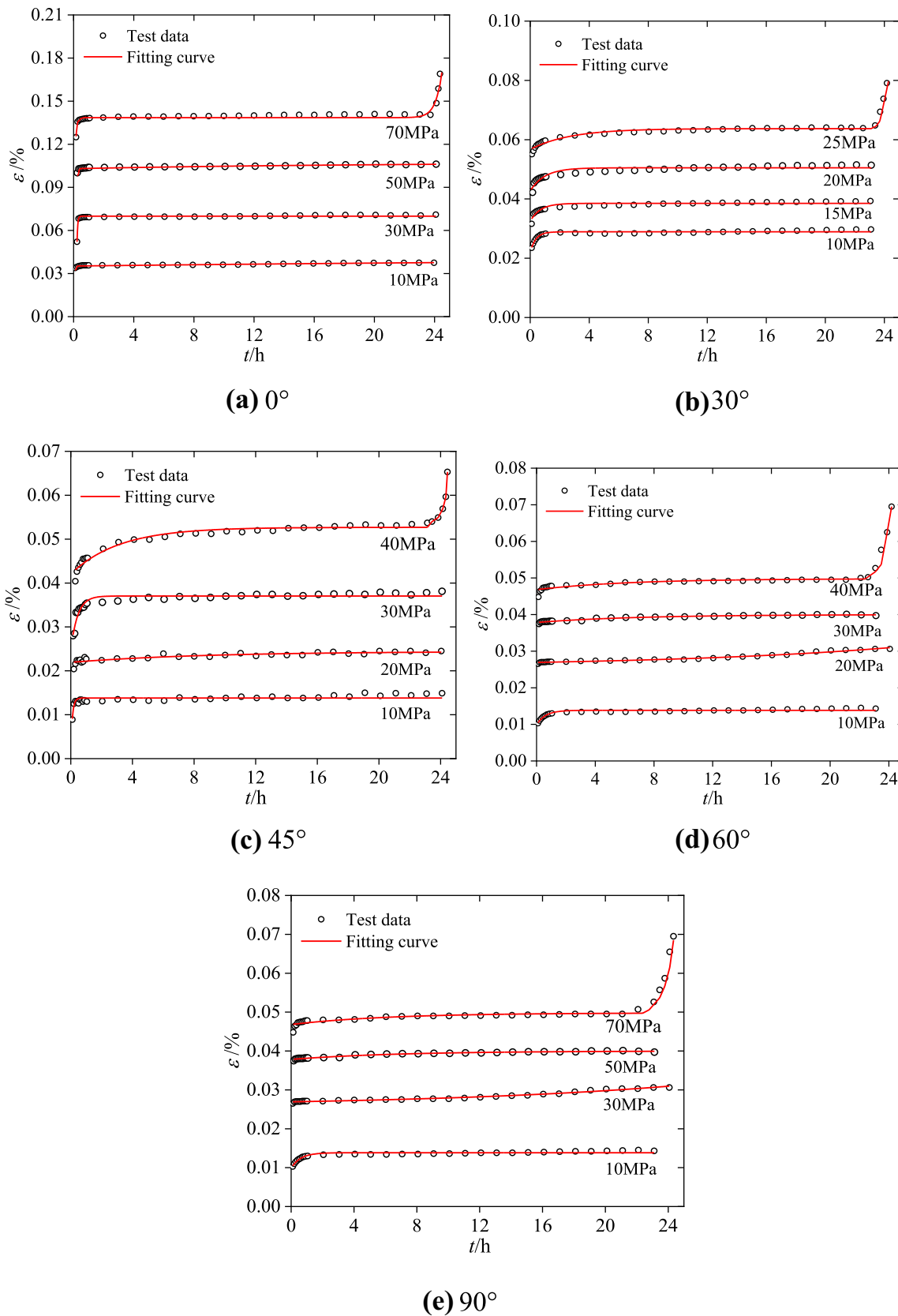| Bedding angle (°) | Stress level (MPa) | $E_M$ (GPa) | $\eta_M$(GPa·h) | $E_K$ (GPa) | $\eta_K$(GPa·h) | $m_1$ | $\eta_B$ (GPa·h) | $m_2$ | $\alpha$ | $\sigma_s$(MPa) |
|---|---|---|---|---|---|---|---|---|---|---|
| 0 | 10 | 127.43 | 972.12 | 77.36 | 140.83 | 0.308 | — | — | — | 66.19 |
| | 30 | 153.01 | 875.48 | 82.12 | 142.72 | 0.397 | — | — | — | |
| | 50 | 163.29 | 861.29 | 86.11 | 128.31 | 0.455 | — | — | — | |
| | 70 | 165.71 | 762.16 | 99.03 | 112.60 | 0.584 | 28.23 | 6.860 | 0.57 | |
| 30 | 10 | 81.94 | 883.04 | 35.34 | 127.49 | 0.286 | — | — | — | 23.80 |
| | 15 | 102.47 | 850.71 | 41.19 | 120.55 | 0.317 | — | — | — | |
| | 20 | 117.83 | 834.63 | 47.64 | 115.31 | 0.384 | — | — | — | |
| | 25 | 128.46 | 814.22 | 53.34 | 112.57 | 0.427 | 35.42 | 6.611 | 0.82 | |
| 45 | 10 | 84.15 | 811.04 | 47.63 | 124.38 | 0.317 | — | — | — | 37.45 |
| | 20 | 88.56 | 803.59 | 51.26 | 113.02 | 0.341 | — | — | — | |
| | 30 | 93.47 | 776.31 | 58.07 | 105.70 | 0.369 | — | — | — | |
| | 40 | 98.23 | 750.48 | 69.50 | 98.66 | 0.391 | 31.07 | 6.403 | 0.79 | |
| 60 | 10 | 96.42 | 837.51 | 49.23 | 113.25 | 0.290 | — | — | — | 38.29 |
| | 20 | 98.30 | 822.13 | 61.3 | 108.44 | 0.306 | — | — | — | |
| | 30 | 107.53 | 806.59 | 70.01 | 96.80 | 0.372 | — | — | — | |
| | 40 | 128.64 | 790.15 | 78.63 | 92.37 | 0.450 | 24.55 | 6.211 | 0.75 | |
| 90 | 10 | 130.12 | 955.27 | 72.23 | 137.55 | 0.315 | — | — | — | 68.41 |
| | 30 | 138.66 | 914.73 | 79.71 | 134.76 | 0.384 | — | — | — | |
| | 50 | 143.52 | 908.45 | 85.35 | 126.84 | 0.431 | — | — | — | |
| | 70 | 160.24 | 879.16 | 97.53 | 124.31 | 0.583 | 35.41 | 6.941 | 0.59 | |

**Fig. 12** Creep data of slate with different bedding angles after 80 F-T cycles and fitting results of the creep damage model: (**a**) 0°, (**b**)30°, (**c**) 45°, (**d**) 60°, (**e**) 90°

**Table 5** Determination results of creep parameters of slate

| Stress level (MPa) | $E_M$ (GPa) | $\eta_M$ (GPa·h) | $E_K$ (GPa) | $\eta_K$ (GPa·h) | $m_1$ | $\eta_B$ (GPa·h) | $m_2$ | $\alpha$ |
|---|---|---|---|---|---|---|---|---|
| 20 | 22.33 | 370.8 | 5.18 | 4459.2 | 0.252 | — | — | — |
| 25 | 20.23 | 221.4 | 16.06 | 2104.2 | 0.273 | — | — | — |
| 30 | 19.81 | 3412.2 | 5.72 | 3455.4 | 0.359 | 457.09 | 5.631 | 0.51 |

curve and the test data fit well, and the fitting coefficients are both greater than 0.9. The model fitting curve reflects the characteristics of decelerating creep, steady-state creep, and accelerated creep stage under different bedding angles and different stress. This verifies the accuracy and applicability of the freeze–thaw and bedding coupling damaged creep constitutive model established in this study.

## Prediction of test results for slate

To further illustrate the rationality of the model proposed in this study, the slate creep test results provided by Mao et al. (2006) are used to further verify the model. The determination results of the model parameters are shown in Table 5. Figure 13 shows the comparison between the theoretical curve of the model and the experimental results. It can be seen that the theoretical curve of the model is in good agreement with the experimental results, indicating that the model can well characterize the creep mechanical properties of slate, which also proves the rationality of the model in this study.
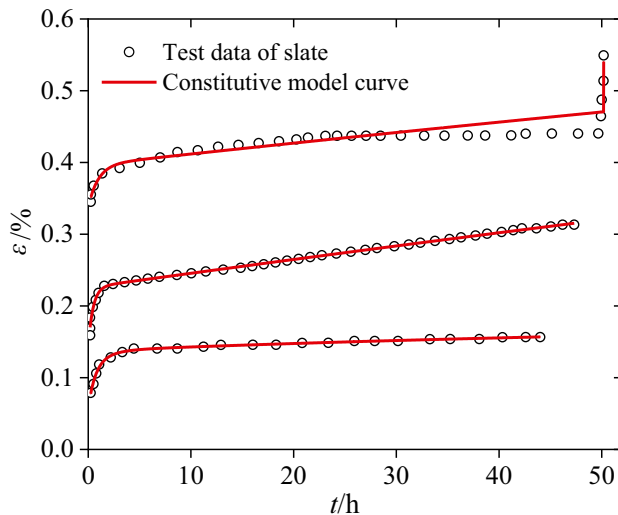


**Fig. 13** Comparison between the theoretical curve and test data of slate

## Discussion

### Influence of the stress level on model parameters

Figure 14 shows the effect of stress level on creep parameters of $E_M$, $\eta_M$, $E_K$, $\eta_K$ and $m_1$, respectively. It can be seen that parameters $E_M$ and $E_K$ increase with the increase in stress level. However, parameters $\eta_M$ and $\eta_K$ decrease with the increase in stress level. The value of fractional order $m_1$ increases with the increase in stress level. That is, the creep rate of the creep curve increases with the increase of stress. Under the action of axial stress, the stress damage of slate increases with the increase of creep time. Under the action of the last stage stress, the creep rate of the slate sample is the largest, so the fractional-order $m_1$ is the largest. When the sample fails, the creep rate increases significantly, and the creep curve enters the accelerated creep stage.

It can be seen from the above that parameters $E_M$ and $E_K$ increase with the increase of stress level, while parameters $\eta_M$ and $\eta_K$ decrease with the increase of stress level. The fractional-order $m_1$ reflects the creep rate of rock in the creep process. At the maximum stress level, when $\beta$ is 60°, the value of $m_1$ is the largest. That is to say, before the accelerated creep stage, the creep characteristics of rock samples with $\beta = 60°$ are the most obvious.

### Influence of viscosity coefficient $\eta_B$ and the fractional derivative $m_2$

Figure 15 shows the influence of bedding angles on the viscosity coefficient $\eta_B$ and the fractional derivative $m_2$. It can be seen from Fig. 15 that with the increase of bedding angle, the changing trend of model parameters $\eta_B$ and $m_2$ first decreases and then increases. When $\beta$ is 60°, these two parameters are the smallest. That is, the corresponding cohesive force $c$ and internal friction angle $\varphi$ are also the smallest, and the shear strength of the sample is also the smallest.
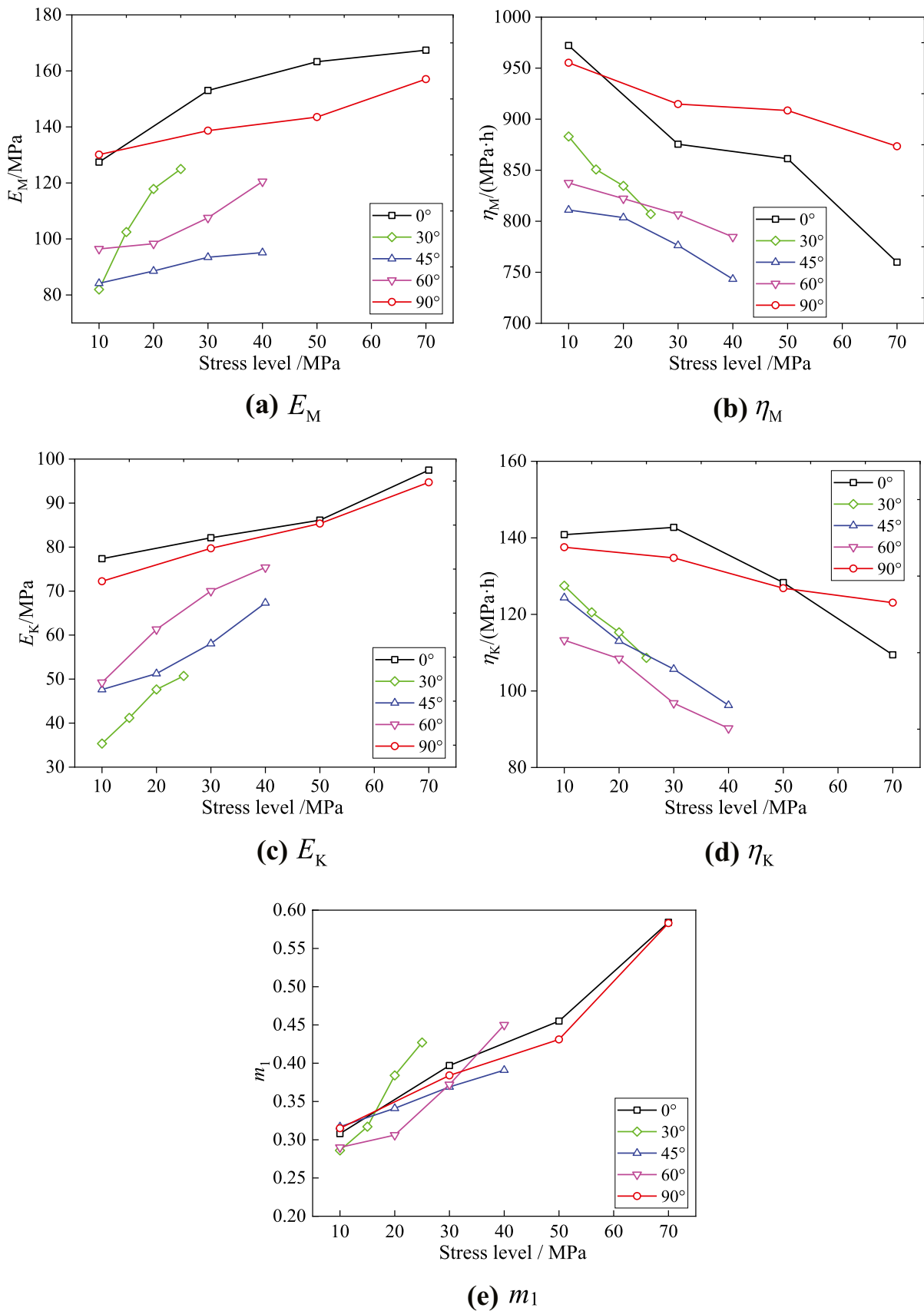
**(a)** $E_M$



**(b)** $\eta_M$



**(c)** $E_K$



**(d)** $\eta_K$



**(e)** $m_1$

**Fig. 14** Influence of the stress level on model parameters of (**a**) $E_M$, (**b**) $\eta_M$, (**c**) $E_K$, (**d**) $\eta_K$, (**e**) $m_1$
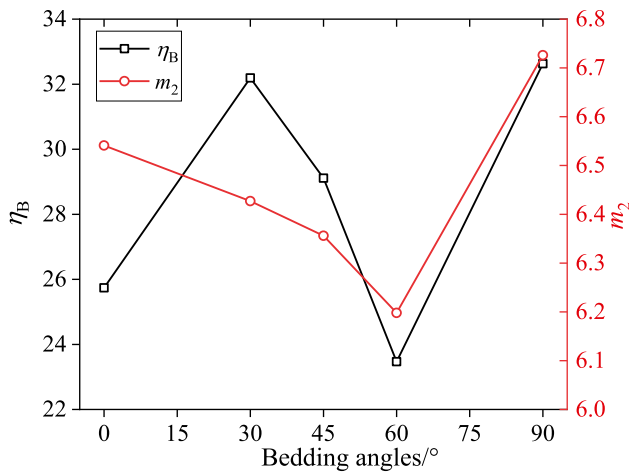
**Fig. 15** Influence of bedding angles on model parameters:$\eta_B$ and $m_2$

# Conclusion

To study the creep characteristics of bedding slates under different freeze–thaw cycles, a series of triaxial creep tests were carried out. Then, based on freeze–thaw and bedding coupling damage and fractional calculus theory, a creep constitutive model considering freeze–thaw damage and bedding damage was established. The main conclusions are as follows:

1. The test results show that the number of freeze-thaw cycles and the bedding angle have a significant effect on the creep behavior of the slate. The creep curve gradually changed from two-stage steady-state creep to three-stage unsteady-state creep, and finally accelerated creep. Under certain bedding angles, the instantaneous deformation, creep deformation, axial initial creep rate, and the steady-state creep rate of slate increase with the increase of freeze-thaw cycles and axial stress.

2. According to the nonlinear rheological theory and fractional calculus theory, considering the freeze-thaw damage and bedding damage, a creep damage model which can simultaneously describe the instantaneous elastic strain, vicious strain, nonlinear viscoelastic strain, and nonlinear viscoplastic strain of freeze-thaw bedding slate is established in this study. Then, the one-dimensional fractional differential creep damage model is derived to three-dimensional. Finally, a simple and feasible method of model parameter identification is given. The experimental verification shows that the model can effectively express the influence of the bedding angles and the freeze-thaw cycles on the creep characteristics of slate, and it can well reflect the nonlinear creep characteristics of the acceleration stage of slate.

3. Through the sensitive analysis of the creep characteristic parameters in the creep damage model, it is found that as the stress level increases, $E_M$ and $E_K$ gradually increases, while $\eta_M$ and $\eta_K$ gradually decrease. The faster the axial strain increases after the rock enters the accelerated creep stage, the shorter the time of the tendency to fail. In addition, with the increase of the bedding angle, the changing trend of the model parameters $\eta_B$ and $m_2$ first decreases and then increases.

# References

Al-Omari A, Beck K, Brunetaud X, Toeroek A, Al-Mukhtar M (2015) Critical degree of saturation: A control factor of freeze-thaw damage of porous limestones at Castle of Chambord. France Engineering Geology 185(5):71–80

Bai Y, Shan R, Han T, Dou H, Liu Z (2021) Study on triaxial creep behavior and the damage constitutive model of red sandstone containing a single ice-filled flaw. Int J Damage Mech 30(3):349–373

Boukharov GN, Chanda MW, Boukharov NG (1995) The three processes of brittle crystalline rock creep. Int J Rock Mech Min Sci Geomech Abstr 32(4):325–335

Chen C, Xu T, Heap MJ, Baud P (2018) Influence of unloading and loading stress cycles on the creep behavior of Darley Dale Sandstone. Int J Rock Mech Min Sci 112(12):55–63

Cong L, Hu X (2017) Triaxial rheological property of sandstone under low confining pressure. Eng Geol 231(12):45–55

Cornet JS, Dabrowski M (2018) Nonlinear Viscoelastic Closure of Salt Cavities. Rock Mech Rock Eng 51(10):3091–3109

Damjanac B, Fairhurst C (2010) Evidence for a Long-Term Strength Threshold in Crystalline Rock. Rock Mech Rock Eng 43:513–531

Feng W, Qiao C, Niu S, Yang Z, Wang T (2020) An improved nonlinear damage model of rocks considering initial damage and damage evolution. Int J Damage Mech 29(7):1117–1137

Fu H, Zhang J, Huang Z, Shi Y, Chen W (2018) A statistical model for predicting the triaxial compressive strength of transversely isotropic rocks subjected to freeze-thaw cycling. Cold Reg Sci Technol 145(1):237–248

Ghobadi MH, Babazadeh R (2015) Experimental Studies on the Effects of Cyclic Freezing-Thawing, Salt Crystallization, and Thermal Shock on the Physical and Mechanical Characteristics of Selected Sandstones. Rock Mech Rock Eng 48(3):1001–1016

Gökçe MV, İnce İ, Fener M, Taşkıran T, Kayabali K (2016) The effects of freeze–thaw (F–T) cycles on the Gödene travertine sed in historical structures in Konya (Turkey). Cold Reg Sci Technol 127(7):65–75

Gutiérrez-Ch JG, Senent S, Estebanez E, Jimenez R (2021) Discrete element modelling of rock creep behaviour using rate process theory. Can Geotech J 58(8):1231–1246

Hale PA, Shakoor A (2003) A Laboratory Investigation of the Effects of Cyclic Heating and Cooling, Wetting and Drying, and Freezing

and Thawing on the Compressive Strength of Selected Sandstones. Environ Eng Geosci 9(2):117–130

Hou R, Kai Z, Jing T, Xue X, Chen Y (2018) A nonlinear creep damage coupled model for rock considering the effect of initial damage. Rock Mech Rock Eng 52(2):1–11

Hu B, Yang SQ, Xu P, Cheng JL (2019) Cyclic loading–unloading creep behavior of composite layered specimens. Acta Geophys 67(2):449–464

Jamshidi A, Nikudel MR, Khamehchiyan M (2016) Evaluation of the durability of Gerdoee travertine after freeze–thaw cycles in fresh water and sodium sulfate solution by decay function models. Eng Geol 202(3):36–43

Jia H, Ding S, Wang Y, Zi F, Sun Q, Yang G (2019) An NMR-based investigation of pore water freezing process in sandstone. Cold Reg Sci Technol 168(12):102893

Jin H (2010) Design and construction of a large-diameter crude oil pipeline in Northeastern China A special issue on permafrost pipeline. Cold Reg Sci Technol 64(3):209–212

Kabwe E, Karakus M, Chanda EK (2020) Creep constitutive model considering the overstress theory with an associative viscoplastic flow rule. Comput Geotech 124(8):103629

Kawamura S, Miura S (2013) Rainfall-induced failures of volcanic slopes subjected to freezing and thawing. Soils Found 53(3):443–461

Khanlari G, Sahamieh RZ, Abdilor Y (2015) The effect of freeze–thaw cycles on physical and mechanical properties of Upper Red Formation sandstones, central part of Iran. Arab J Geosci 8(8):5991–6001

Kilbas AA, Srivastava HM, Trujillo JJ, Van Mill J (2006) Theory and applications of fractional differential equations. Elsevier Science B.V, Amsterdam

Knutsson R, Viklander P, Knutsson S, Laue J (2018) How to avoid permafrost while depositing tailings in cold climate. Cold Reg Sci Technol 153(9):86–96

Kodama J, Mitsui Y, Fukuda D (2019) Time-dependence of mechanical behavior of Shikotsu welded tuff at sub-zero temperatures. Cold Reg Sci Technol 168(12):102868

Kuhn MR, Mitchell JK (1992) Modelling of soil creep with the discrete element method. Eng Comput 9(2):277–287

Landel RF, Nielsen LE (1993) Mechanical Properties of Polymers and Composites. Marcel Dekker, New York

Lee YK, Pietruszczak S (2008) Application of critical plane approach to the prediction of strength anisotropy in transversely isotropic rock masses. Int J Rock Mech Min Sci 45(4):513–523

Liu J, Jing H, Meng B, Wang L, Zhang X (2020) A four-element fractional creep model of weakly cemented soft rock. Bull Eng Geol Env 79(10):5569–5584

Ma JZ, Zhang J, Huang HW, Zhang LL, Huang JS (2017) Identification of representative slip surfaces for reliability analysis of soil slopes based on shear strength reduction. Comput Geotech 85(5):199–206

Mao HJ, Yang CH, Liu J, Wang XC (2006) Testing study and modeling analysis of creep behavior of slates. Chin J Rock Mech Eng 25(6):1204–1209

Main IG (2010) A damage mechanics model for power-law creep and earthquake aftershock and foreshock sequences. Geophys J Roy Astron Soc 142(1):151–161

Ngwenya BT, Main IG, Elphick SC, Crawford BR, Smart B (2001) A constitutive law for low-temperature creep of water-saturated sandstones. Journal of Geophysical Research Solid Earth 106(B10):21811–21826

Rassouli FS, Zoback M (2018) Comparison of Short-Term and Long-Term Creep Experiments in Shales and Carbonates

from Unconventional Gas Reservoirs. Rock Mech Rock Eng 51(7):1995–2014

Shi Y, FU H, Wu Y, Deng H (2020) Study on damage constitutive model of layered rock under uniaxial compression. Journal of Huazhong University of Science and Technology (natural Science Edition) 48(09):126–132

Sun Y, Zhai C, Xu J, Cong Y, Qin L, Zhao C (2020) Characterisation and evolution of the full size range of pores and fractures in rocks under freeze-thaw conditions using nuclear magnetic resonance and three-dimensional X-ray microscopy. Eng Geol 271(6):105616

Wang D, Chen G, Jian D, Zhu J, Lin Z (2021) Shear creep behavior of red sandstone after freeze-thaw cycles considering different temperature ranges. Bull Eng Geol Env 80(3):2349–2366

Wang J, Zhang Q, Song Z, Zhang Y (2019) Creep properties and damage constitutive model of salt rock under uniaxial compression. Int J Damage Mech 29(6):902–922

Wang P, Xu J, Liu S, Wang H, Liu S (2016) Static and dynamic mechanical properties of sedimentary rock after freeze-thaw or thermal shock weathering. Eng Geol 210(4):148–157

Yang X, Jiang A, Li M (2019) Experimental investigation of the time-dependent behavior of quartz sandstone and quartzite under the combined effects of chemical erosion and freeze–thaw cycles. Cold Reg Sci Technol 161(5):51–62

Yang X, Jiang A, Zhang F (2021) Research on creep characteristics and variable parameter-based creep damage constitutive model of gneiss subjected to freeze–thaw cycles. Environmental Earth Sciences 80(1):7–15

Yang Y, Lai Y, Li J (2010) Laboratory investigation on the strength characteristic of frozen sand considering effect of confining pressure. Cold Reg Sci Technol 60(3):245–250

Yavuz H (2011) Effect of freeze-thaw and thermal shock weathering on the physical and mechanical properties of an andesite stone. Bull Eng Geol Env 70(2):187–192

Yin D, Wu H, Cheng C, Chen Y (2013) Fractional order constitutive model of geomaterials under thecondition of triaxial test. Int J Numer Anal Meth Geomech 37(8):961–972

Zhang Q, Yang W, Zhang J, Yang C (2009) Variable parameters-based creep damage constitutive model and its engineering application. Chin J Rock Mech Eng 28(4):732–739

Zhang Y, Shao J, Xu W, Jia Y (2016) Time-Dependent Behavior of Cataclastic Rocks in a Multi-Loading Triaxial Creep Test. Rock Mech Rock Eng 49(9):3793–3803

Zhang C, Zou P, Wang Y (2020a) An elasto-visco-plastic model based on stress functions for deformation and damage of water-saturated rocks during the freeze-thaw process. Constr Build Mater 250(8):402–411

Zhang H, Meng X, Yang G (2020b) A study on mechanical properties and damage model of rock subjected to freeze-thaw cycles and confining pressure. Cold Reg Sci Technol 174(6):103056

Zhang H, Min C, Xiangrui Q (2021) Constitutive model of rock mass considering initial joint damage. Mining Research and Development 41(10):73–78

Zhang J, Fu H, Huang Z, Wu Y, Chen W, Shi Y (2019a) Experimental study on the tensile strength and failure characteristics of transversely isotropic rocks after freeze-thaw cycles. Cold Reg Sci Technol 163(7):68–77

Zhang X, Ou X, Gong F, Yang J (2019b) Effects of Bedding on The Dynamic Compressive Properties of Low Anisotropy Slate. Rock Mech Rock Eng 52(4):981–990

Zhou HW, Wang CP, Han BB, Duan ZQ (2011) A creep constitutive model for salt rock based on fractional derivatives. Int J Rock Mech Min Sci 48(1):116–121